Two-dimensional Heisenberg model with material-dependent superexchange interactions

Jia-Wen Li,[1] Zhen Zhang,[2] Jing-Yang You,[3] Bo Gu,[1,4,5,*] and Gang Su[1,4,5,6,†]

[1]*Kavli Institute for Theoretical Sciences, University of Chinese Academy of Sciences, Beijing 100049, China*

[2]*Key Laboratory of Multifunctional Nanomaterials and Smart Systems, Division of Advanced Materials, Suzhou Institute of Nano-Tech and Nano-Bionics, Chinese Academy of Sciences, Suzhou 215123, China*

[3]*Department of Physics, National University of Singapore, 2 Science Drive 3, Singapore 117551*

[4]*CAS Center for Excellence in Topological Quantum Computation, University of Chinese Academy of Sciences, Beijing 100190, China*

[5]*Physical Science Laboratory, Huairou National Comprehensive Science Center, Beijing 101400, China*

[6]*School of Physical Sciences, University of Chinese Academy of Sciences, Beijing 100049, China*

(Received 4 January 2023; revised 8 April 2023; accepted 16 May 2023; published 12 June 2023)

The two-dimensional (2D) van der Waals ferromagnetic semiconductors, such as CrI_3 and $Cr_2Ge_2Te_6$, and the 2D ferromagnetic metals, such as Fe_3GeTe_2 and $MnSe_2$, have been obtained in recent experiments and attracted a lot of attention. The superexchange interaction has been suggested to dominate the magnetic interactions in these 2D magnetic systems. In the usual theoretical studies, the expression of the 2D Heisenberg models were fixed by hand due to experiences. Here, we propose a procedure to determine the expression of the 2D Heisenberg models by counting the possible superexchange paths with the density functional theory and Wannier function calculations. With this method, we obtain a 2D Heisenberg model with six different nearest-neighbor exchange coupling constants for the 2D ferromagnetic metal Cr_3Te_6, which is very different for the crystal structure of Cr atoms in Cr_3Te_6. The calculated Curie temperature Tc = 328 K is close to the Tc = 344 K of 2D Cr_3Te_6 reported in recent experiment. In addition, we predict two stable 2D ferromagnetic semiconductors Cr_3O_6 and Mn_3O_6 sharing the same crystal structure of Cr_3Te_6. The similar Heisenberg models are obtained for 2D Cr_3O_6 and Mn_3O_6, where the calculated Tc is 218 K and 208 K, respectively. Our paper offers a practical approach to determine the expression of Heisenberg models for these 2D magnetic semiconductors and metals, and builds up a solid basis for further studies.

DOI: 10.1103/PhysRevB.107.224411

I. INTRODUCTION

Recently, the successful synthesis of two-dimensional (2D) van der Waals ferromagnetic semiconductors in experiments, such as CrI_3 [1] and $Cr_2Ge_2Te_6$ [2] has attracted extensive attention to 2D ferromagnetic materials. According to Mermin-Wagner theorem [3], the magnetic anisotropy is essential to produce the long-range magnetic order in 2D systems. For the 2D magnetic semiconductors obtained in experiments, the Curie temperature Tc is still much lower than room temperature[1,2,4–9], as listed in Table I. For applications, the ferromagnetic semiconductors with Tc higher than room temperature are highly required [10–13]. On the other hand, many 2D van der Waals ferromagnetic metals with high Tc have been obtained in recent experiments [14–25], as shown in Table II.

In these 2D van der Waals ferromagnetic materials, the superexchange interaction has been suggested to dominate the magnetic interactions. The superexchange interaction describes the indirect magnetic interaction between two magnetic cations mediated by the neighboring nonmagnetic anions [26–28]. The superexchange interaction has been discussed in the 2D magnetic semiconductors. Based on the superexchange interaction, the strain-enhanced Tc in 2D ferromagnetic semiconductor $Cr_2Ge_2Se_6$ can be understood by the decreased energy difference between the d electrons of cation Cr atoms and the p electrons of anion Se atoms [29]. The similar superexchange picture was obtained in several 2D ferromagnetic semiconductors, including the great enhancement of Tc in bilayer heterostructures $Cr_2Ge_2Te_6/PtSe_2$ [30], the high Tc in technetium-based semiconductors $TcSiTe_3$, $TcGeSe_3$, and $TcGeTe_3$ [31], and the electric field enhanced Tc in the monolayer $MnBi_2Te_4$ [32]. The superexchange interaction has also been discussed in the semiconductor heterostructure $CrI_3/MoTe_2$ [33], and 2D semiconductor $Cr_2Ge_2Te_6$ with molecular adsorption [34].

In addition, the superexchange interaction has also been obtained in the 2D van der Waals ferromagnetic metals. By adding vacancies, the angles of the superexchange interaction paths of 2D metals VSe_2 and $MnSe_2$ will change, thereby tuning the superexchange coupling strength [35]. It is found that biaxial strain changes the angle of superexchange paths in 2D metal Fe_3GeTe_2, and affects Tc [36]. Under tensile strain, the ferromagnetism of the 2D magnetic metal CoB_6 is enhanced, due to the competition between superexchange and direct exchange interactions [37].

It is important to determine the spin Hamiltonian for the magnetic materials, in order to theoretically study the

*gubo@ucas.ac.cn
†gsu@ucas.ac.cn

TABLE I. Experimental results of Curie temperature of 2D ferromagnetic semiconductors.

Semiconductors	Tc (K)	Reference of experiments
CrI_3	45	Ref. [1] (2017)
$Cr_2Ge_2Te_6$	30	Ref. [2] (2017)
$CrBr_3$	34	Ref. [4] (2019)
$CrCl_3$	17	Ref. [5] (2019)
Cr_2S_3	75	Refs. [6,7] (2019)
$CrSiTe_3$	80	Ref. [8] (2021)
CrSBr	146	Ref. [9] (2021)

magnetic properties, such as Tc. In the usual theoretical studies, the expression of the spin Hamiltonian needs to be fixed by hand according to the experiences. By the four-state method and density functional theory (DFT) calculations [38–40], the exchange coupling parameters of the spin Hamiltonian, such as the nearest neighbor, the next nearest neighbor, interlayer, etc., can be obtained. Then the Tc can be estimated through Monte Carlo simulations [40,41]. With different spin Hamiltonians chosen by hand, sometimes different results are obtained in calculations. Is it possible to determine the spin Hamiltonian by the help of calculations rather than by the experiences?

In this paper, we propose a procedure to establish the 2D Heisenberg models for the 2D van der Waals magnetic materials, when the superexchange interactions dominate. Through the DFT and Wannier function calculations, we can calculate the exchange coupling between any two magnetic cations, by counting the possible superexchange paths. By this approach, we obtain a 2D Heisenberg model with six different nearest-neighbor exchange coupling constants for the 2D van der Waals ferromagnetic metal Cr_3Te_6 [17], where the calculated Tc = 328 K is close to the Tc = 344 K reported in the experiment. In addition, based on the crystal structure of 2D Cr_3Te_6, we predict two 2D magnetic semiconductors Cr_3O_6 and Mn_3O_6 with Tc of 218 and 208 K, and energy gap of 0.99 and 0.75 eV, respectively.

II. COMPUTATIONAL METHODS

Our calculations were based on the DFT as implemented in the Vienna *ab initio* simulation package (VASP) [42]. The exchange-correlation potential is described with the Perdew-Burke-Ernzerhof (PBE) form of the generalized gradient approximation (GGA) [43]. The electron-ion potential is described by the projector-augmented wave (PAW) method [44]. We carried out the calculation of GGA + U with $U = 3.2$ eV, a reasonable U value for the 3d electrons of Cr in Cr_3Te_6 [17]. The band structures for 2D Cr_3O_6 and Mn_3O_6 were calculated in HSE06 hybrid functional [45]. The plane-wave cutoff energy is set to be 500 eV. Spin polarization is taken into account in structure optimization. To prevent interlayer interaction in the supercell of 2D systems, the vacuum layer of 16 is included. The $5 \times 9 \times 1$, $5 \times 9 \times 1$, and $7 \times 11 \times 1$ Monkhorst Pack k-point meshed were used for the Brillouin zone (BZ) sampling for 2D Cr_3O_6, Cr_3Te_6, and Mn_3O_6, respectively [46]. The structures of 2D Cr_3O_6 and Mn_3O_6 were fully relaxed, where the convergence precision of energy and force were 10^{-6} and 10^{-3} eV/, respectively. The phonon spectra were obtained in a $3 \times 3 \times 1$ supercell with the PHONOPY package [47]. The WANNIER90 code was used to construct a tight-binding Hamiltonian [48,49] to calculate the magnetic coupling constant. In order to cover all superexchange paths, a $2 \times 2 \times 1$ supercell is used in the tight-binding calculation. In the calculation of molecular dynamics, a $3 \times 4 \times 1$ supercell (108 atoms) was built, and we took the NVT ensemble (constant-temperature, constant-volume ensemble) and maintained a temperature of 250 K with a step size of 3 fs and a total duration of 6 ps.

TABLE II. Experimental results of Curie temperature of 2D ferromagnetic metals.

Metals	Tc (K)	Reference of experiments
CrTe	140	Ref. [14] (2020)
$CrTe_2$	300	Refs. [15,16] (2021)
Cr_3Te_6	344	Ref. [17] (2021)
Cr_3Te_4	160	Ref. [18] (2021)
CrSe	280	Ref. [19] (2019)
Fe_3GeTe_2	300	Refs. [20,21] (2018)
Fe_4GeTe_2	270	Ref. [22] (2020)
Fe_5GeTe_2	229	Ref. [24] (2019)
$MnSe_2$	300	Ref. [25] (2018)

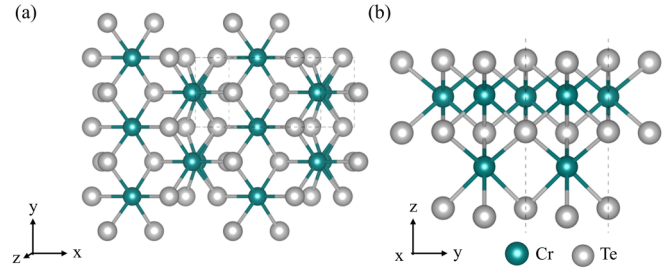

FIG. 1. Crystal structure of Cr_3Te_6. (a) Top view. (b) Side view.

III. PROCEDURE TO DETERMINE THE 2D HEISENBERG MODEL: AN EXAMPLE OF 2D Cr_3Te_6

A. Calculate exchange coupling *J* from superexchange paths

The crystal structure of 2D Cr_3Te_6 is shown in Fig. 1, where the space group is Pm (No. 6). In experiment, it is a ferromagnetic metal with high Tc = 344 K [17]. To theoretically study its magnetic properties, we considered seven different magnetic configurations, including a ferromagnetic (FM), a ferrimagnetic (FIM), and five antiferromagnetic (AFM) configurations, as discussed in Supplemental Material [50]. The calculation results show that the magnetic ground state is ferromagnetic, consistent with the experimental results. Since the superexchange interaction has been suggested to dominate the magnetic interactions in these 2D van der Waals ferromagnetic semiconductors and metals, we study the superexchange interactions in 2D Cr_3Te_6.

The superexchange interaction can be reasonably descried by a simple Cr-Te-Cr model [51], as shown in Fig. 2. There

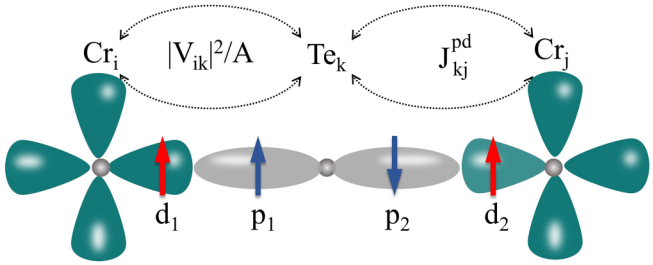

FIG. 2. Schematic picture of superexchange interaction by a Cr-Te-Cr model. There are two processes: One is the direct exchange process between Cr$_j$ and Te$_k$, noted as J^{pd}_{kj}, and the other is electron hopping between Te$_k$ and Cr$_i$, noted as $|V_{ik}|^2/A$. See text for details.

are two Cr atoms at sites i and j, and one Te atom at site k between the two Cr atoms. By the perturbation calculation, the superexchange coupling J_{ij} between the two Cr atoms can be obtained as [51]

$$J_{ij} = \left(\frac{1}{E^2_{\uparrow\downarrow}} - \frac{1}{E^2_{\uparrow\uparrow}}\right) \sum_{k,p,d} |V_{ik}|^2 J^{pd}_{kj} = \frac{1}{A} \sum_{k,p,d} |V_{ik}|^2 J^{pd}_{kj}. \quad (1)$$

The indirect exchange coupling J_{ij} is consisting of two processes. One is the direct exchange process between the d electron of Cr at site j and the p electrons of Te at site k, presented by J^{pd}_{kj}. The other is the electron hopping process between p electrons of the Te atom at site k and d electrons of the Cr atom at site i, presented by $|V_{ik}|^2/A$. V_{ik} is the hopping parameter between d electrons of the Cr atom at site i and p electrons of the Te atom at site k. Here, $A = 1/(1/E^2_{\uparrow\downarrow}\text{-}1/E^2_{\uparrow\uparrow})$, and is taken as a pending parameter. $E_{\uparrow\uparrow}$ and $E_{\uparrow\downarrow}$ are energies of two d electrons at Cr atom at site i with parallel and antiparallel spins, respectively. The direct exchange coupling J^{pd}_{kj} can be expressed as [29–32]

$$J^{pd}_{kj} = \frac{2|V_{kj}|^2}{\left|E^p_k - E^d_j\right|}. \quad (2)$$

V_{kj} is the hopping parameter between p electrons of the Te atom at site k and d electrons of the Cr atom at site j. E^p_k is the energy of p electrons of the Te atom at site k, and E^d_j is the energy of d electrons of the Cr atom at site j.

By the DFT and Wannier function calculations, the parameters V_{ik}, V_{kj}, E^p_k, and E^d_j in Eqs. (1) and (2) can be calculated. The $J_{ij}A$ can be obtained by counting all the possible k sites of Te atoms, p orbitals of Te atoms, and d orbitals of Cr atoms.

From the calculated results in Table III, it is suggested that there are six different nearest-neighbor couplings, denoted as J_{11}, J_{22}, J_{33}, J_{12}, J_{13}, and J_{23}, as shown in Fig. 3(b). Accordingly, there are three kinds of Cr atoms, noted as Cr$_1$, Cr$_2$, and Cr$_3$. Based on the results in Table III, the effective spin Hamiltonian can be written as

$$\begin{aligned} H = {} & J_{11} \sum_n \vec{S}_{1n} \cdot \vec{S}_{1n} + J_{22} \sum_n \vec{S}_{2n} \cdot \vec{S}_{2n} + J_{33} \sum_n \vec{S}_{3n} \cdot \vec{S}_{3n} \\ & + J_{12} \sum_n \vec{S}_{1n} \cdot \vec{S}_{2n} + J_{13} \sum_n \vec{S}_{1n} \cdot \vec{S}_{3n} + J_{23} \sum_n \vec{S}_{2n} \cdot \vec{S}_{3n} \\ & + D \sum_n \left(S^2_{1nz} + S^2_{2nz} + S^2_{3nz}\right), \end{aligned} \quad (3)$$

TABLE III. For 2D Cr_3Te_6, the calculated exchange coupling parameters $J_{ij}A$ in Eqs. (1) and (2), by the density functional theory and Wannier functional calculations. A is a pending parameter. The unit of $J_{ij}A$ is meV^3.

$J_{11}A$	$J_{22}A$	$J_{33}A$	$J_{12}A$	$J_{13}A$	$J_{23}A$
40	26	53	29	44	83

where J_{ij} means magnetic coupling between Cr$_i$ and Cr$_j$, as indicated in Fig. 3(b). D represents the magnetic anisotropy energy (MAE) of Cr_3Te_6.

B. Determine the parameters *D* and *A*

The single-ion magnetic anisotropy parameter DS^2 can be obtained by $DS^2 = (E_\perp\text{-}E_\parallel)/6$, where $E_\perp$ and $E_\parallel$ are energies of Cr_3Te_6 with out-of-plane and in-plane polarizations in the FM state, respectively. It has $DS^2 = -0.14$ meV/Cr for 2D Cr_3Te_6, which is in agreement with the value of -0.13 meV/Cr reported in the previous study of Cr_3Te_6 [17].

The parameter A can be calculated in the following way. Considering FM and AFM configurations, the total energy of Eq. (3) without the MAE term can be, respectively, expressed as [50]

$$\begin{aligned} E_{\rm FM} &= 2J_{11}S_1^2 + 2J_{22}S_2^2 + 2J_{33}S_3^2 + 8J_{12}S_1S_2 \\ &\quad + 2J_{23}S_2S_3 + 8J_{13}S_1S_3 + E_0 \\ &= 11838/A + E_0, \\ E_{\rm AFM1} &= 2J_{11}S_1^2 + 2J_{22}S_2^2 - 2J_{33}S_3^2 - 8J_{12}S_1S_2 + E_0 \\ &= -2502/A + E_0, \end{aligned} \quad (4)$$

where S_1, S_2, S_3 are 3.40, 3.45, and 3.53 μ_B, respectively.

The results in Table III are used to obtain the final expressions in Eq. (4). Since two parameters A and E_0 are kept, two spin configurations FM and AFM1 are considered here. Discussion on the choice of spin configurations is given in Supplemental Material [50]. For the FM spin configuration, the ground state of Cr_3Te_6, the total energy is taken as $E_{\rm FM} = 0$ for the energy reference. The total energy of AFM1, $E_{\rm AFM1} = 535$ meV, is obtained by the DFT calculation. The parameters A and E_0 are obtained by solving Eq. (4), and the six exchange coupling parameters J_{ij} can be obtained by Table III. The results are given in Table IV.

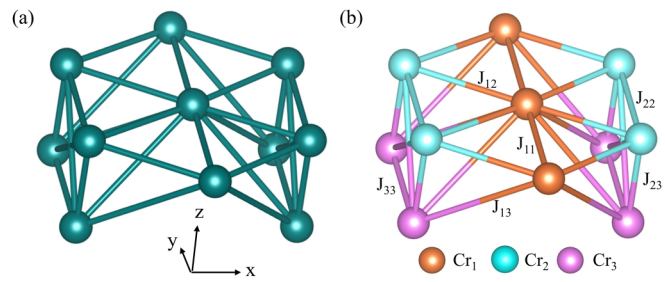

FIG. 3. (a) The crystal structure of Cr atoms in 2D Cr_3Te_6. (b) The magnetic structure of Cr atoms in 2D Cr_3Te_6, calculated by Eqs. (1) and (2).

TABLE IV. For 2D magnetic metal Cr_3Te_6 and semiconductors Cr_3O_6 and Mn_3O_6, the parameter A (in units of meV^{-2}) in Eq. (1), the exchange coupling parameters $J_{ij}S^2$ and the magnetic anisotropy parameter DS^2 (in units of meV) in the Hamiltonian in Eq. (3), and the estimated Curie temperature Tc. See text for details.

Materials	A	$J_{11}S^2$	$J_{22}S^2$	$J_{33}S^2$	$J_{12}S^2$	$J_{13}S^2$	$J_{23}S^2$	DS^2	Tc (K)
Cr_3Te_6	−27	−17.1	−11.5	−24.4	−12.6	−19.6	−37.4	−0.14	328
Cr_3O_6	−36	−18.9	−14.6	−10.1	−18.7	−1.8	−3.1	0.04	218
Mn_3O_6	−465	−11.9	−7.6	−50.4	−15.9	−5.2	−10.7	−0.09	208

C. Estimate Tc by Monte Carlo simulation

To calculate the Curie temperature, we used the Monte Carlo program for the Heisenberg-type Hamiltonian in Eq. (3) with parameters in Table IV. The Monte Carlo simulation was performed on a $30\sqrt{3} \times 30\sqrt{3}$ lattice with more than 1×10^6 steps for each temperature. The first two-third steps were discarded, and the last one-third steps were used to calculate the temperature-dependent physical quantities. As shown in Table IV and Fig. 4(d), the calculated Tc = 328 K for 2D Cr_3Te_6, close to the Tc = 344 K of 2D Cr_3Te_6 in the experiment [17]. Discussion on the choice of spin configurations and the estimation of exchange couplings J_{ij} and Tc is given in Supplemental Material [50].

IV. PREDICTION OF TWO HIGH CURIE TEMPERATURE MAGNETIC SEMICONDUCTORS Cr_3O_6 and Mn_3O_6

Inspired by the high Tc in the 2D magnetic metal Cr_3Te_6, we explore the possible high Tc magnetic semiconductors with the same crystal structure of Cr_3Te_6 by the DFT calculations. We obtain two stable ferromagnetic semiconductors Cr_3O_6 and Mn_3O_6. In order to study the stability of the 2D Cr_3O_6 and Mn_3O_6, we calculate the phonon spectrum. As shown in Supplemental Material [50], there is no imaginary frequency, indicating the dynamical stability. In addition, we performed molecular dynamics simulations of Cr_3O_6 and Mn_3O_6 at 250 K, taking the NVT ensemble (constant temperature and volume) and run for 6 ps. The results show that 2D Cr_3O_6 and Mn_3O_6 are thermodynamically stable [50]. These calculation results suggest that 2D Cr_3O_6 and Mn_3O_6 may be feasible in experiment.

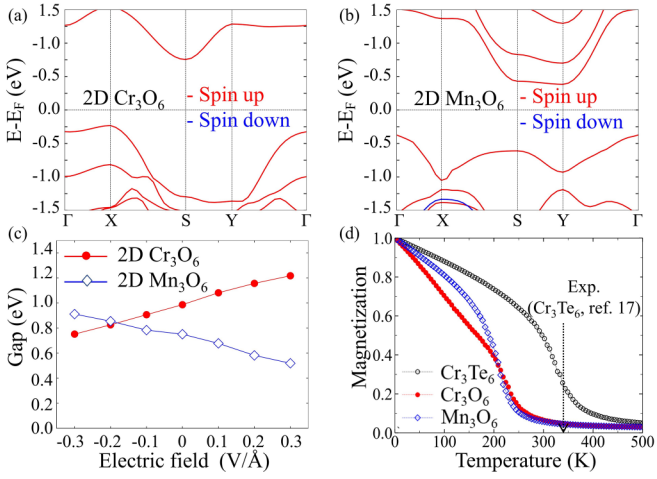

FIG. 4. (a) Band structures of Cr_3O_6 with a bandgap of 0.99 eV. (b) Band structures of Mn_3O_6 with a bandgap of 0.75 eV. (c) Energy gap of Cr_3O_6 and Mn_3O_6 under external electric field out-plane. (d) The magnetic moment of Cr_3Te_6, Cr_3O_6, and Mn_3O_6 varies with temperature.

The band structure of 2D Cr_3O_6 and Mn_3O_6 is shown in Figs. 4(a) and 4(b), respectively, where the band gap is 0.99 eV for Cr_3O_6 and 0.75 eV for Mn_3O_6. As shown in Figs. 4(a) and 4(b), the band gap for 2D Cr_3O_6 and Mn_3O_6 is 0.99 eV and 0.75 eV, respectively. When applying an out-of-plane electric field with a range of ±0.3 V/nm, which is possible in experiment [52], the band gap of Cr_3O_6 (Mn_3O_6) increases (decreases) with increasing electric field, as shown in Fig. 4(c). By the same calculation method above, the parameter A, the similar Heisenberg models in Eq. (3) with six nearest-neighbor exchange coupling J_{ij} are obtained for the 2D Cr_3O_6 and Mn_3O_6. The parameters A, J_{ij}, and D are calculated and shown in Table IV. The spin polarization of Cr_3O_6 and Mn_3O_6 is in-plane ($DS^2 = 0.04$ meV) and out-of-plane ($DS^2 = -0.09$ meV), respectively. Figure 4(d) shows the magnetization as a function of temperature for 2D Cr_3Te_6, Cr_3O_6, and Mn_3O_6. The calculated Curie temperature is Tc = 218 K for 2D Cr_3O_6 and Tc = 208 K for 2D Mn_3O_6, respectively.

According to the Mermin-Wagner theorem [3], at finite temperatures, the 2D isotropic Heisenberg model will not have the long-range magnetic orders at finite temperatures. Thus, to stabilize long-range ferromagnetic order in 2D magnetic semiconductors at finite temperature, a large magnetic anisotropy, which makes the systems away from the 2D isotropic Heisenberg model, is essentially important. In fact, some 2D magnetic materials with in-plane magnetization have been obtained experimentally, such as 2D $CrCl_3$ [5] and 2D CrSBr [9]. It is noted that the materials considered in this paper have low symmetry and therefore are likely to have a preferred direction within the plane which eventually allows the system to have a long-range magnetic order.

V. DISCUSSION

A. Effect of strain on magnetism of 2D Cr_3Te_6

In order to study the effect of lattice variations, we calculate the hopping parameter and the energy difference between the FM and AFM1 states E_{AFM1}-E_{FM} by applying the isotropic strain. The numerical results are shown in Fig. 5. Some of the strongest hopping parameters between the Cr and Te atoms in 2D Cr_3Te_6 are shown in Fig. 5(a). It is shown that these hopping parameters are decreased with the increasing lattice constant, which is well expected. On the other hand, the energy difference E_{AFM1}-E_{FM} is increased and the FM state

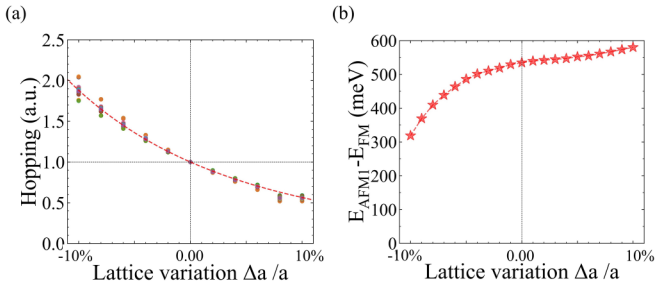

FIG. 5. Effect of lattice variations on the hopping parameters and the FM state in 2D Cr_3Te_6. (a) Some of the strongest hopping parameters between the Cr and Te atoms in 2D Cr_3Te_6 with lattice variations. (b) Energy difference between the FM and AFM1 states in 2D Cr_3Te_6 with lattice variations.

becomes stronger with the increasing lattice constant. Thus, it is difficult to understand the FM states in 2D Cr_3Te_6 with lattice variations only in terms of the hopping parameters.

In order to understand the FM state in 2D Cr_3Te_6 with lattice variations, we study the energy level E_d of the 3d orbitals of Cr atoms and the E_p of the 5p orbitals of the nearest Te atoms in 2D Cr_3Te_6, and the hopping matrix element $|V_{pd}|$ between the 3d orbitals of Cr atoms and the 5p orbitals of the nearest Te atoms. The supercell used in calculation is shown in Fig. 6. As shown in Table V, with the increasing lattice constant, some of the energy differences $|E_p - E_d|$ are dramatically decreased, while the hopping matrix element $|V_{pd}|$ are slightly decreased. These results suggest the superexchange mechanism, where the indirect ferromagnetic coupling between Cr atoms is proportional to the factor $|V_{pd}|^4/|E_p - E_d|$, as shown in Eqs. (1) and (2) in the paper. For the increasing lattice constant, some of the energy differences $|E_p - E_d|$ are dramatically decreased, the hopping matrix element $|V_{pd}|$ are slightly decreased, the corresponding factors $|V_{pd}|^4/|E_p - E_d|$ are increased, and thus the ferromagnetic coupling between Cr atoms is increased.

B. Effect of U on magnetism of 2D Cr_3Te_6

We calculate the energy difference between the ferromagnetic (FM) and the antiferromagnetic (AFM1) states E_{AFM1}-E_{FM} with parameters of $U = 0 \sim 5$ eV and HSE06, respectively. As shown in Fig. 7, the energy difference E_{AFM1}-E_{FM} is increased and the FM state becomes stronger with the increasing parameter U, which is reasonable and expected. In addition, the result with parameter HSE06 gives

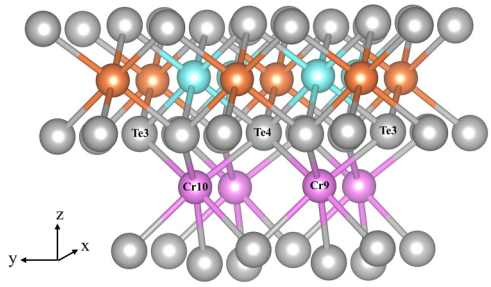

FIG. 6. Schematic crystal structure of 2D Cr_3Te_6, where the Cr and Te atoms discussed in Table V are noted.

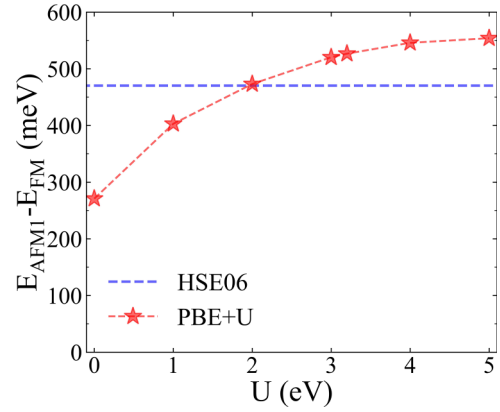

FIG. 7. Energy difference between the FM and AFM1 states in 2D Cr_3Te_6 with parameters of $U = 0 \sim 5$ eV and HSE06, respectively.

an energy difference of 470 meV, close to the result with parameter $U = 2$ eV. For the 3d orbitals, the parameters $U = 2 \sim 5$ eV are reasonable values, and the $U = 3.2$ eV is used in our paper.

C. Discussion about our approach

In the conventional method to calculate Tc, there are three steps. One, choose a kind of spin Hamiltonian by hand due to experience. Two, estimate the exchange coupling by DFT calculations [38–40], which depends on the choice of magnetic configurations. Three, estimate Tc of the spin Hamiltonian by classic Monte Carlo simulations. Our point in the paper is to improve the conventional step one. We propose a procedure to determine the expression of the 2D Heisenberg models by DFT calculations, when the superexchange interaction is dominated. For the superexchange coupling J_{ij} as shown in Eq. (1), there is a parameter A defined as $1/A = (1/E^2_{\uparrow\downarrow}$-$1/E^2_{\uparrow\uparrow})$, where $E_{\uparrow\downarrow}$ and $E_{\uparrow\uparrow}$ are energies of the Cr atom with antiparallel or parallel electron spin state [51]. Since it's difficult to obtain $E_{\uparrow\downarrow}$ and $E_{\uparrow\uparrow}$ by DFT calculation, A is treated as a pending parameter. In order to obtain A, we follow the conventional step two, which indeed depends on the choice of magnetic configurations, as shown in Table I in Supplemental Material [50]. For the spin configurations of FM and AFM1 for 2D Cr_3Te_6, the calculated $A = -27$ meV^2 and Tc = 328 K, which is close to the Tc = 344 K of 2D Cr_3Te_6 in the experiment [17].

Here, we note the difference between our approach and the previous theoretical studies with the superexchange picture. To understand the increased Tc of 2D magnetic semiconductor $Cr_2Ge_2Se_6$ under strain, the AFM exchange coupling J^{pd} between the d orbitals of Cr atoms and the p orbitals of nearby Se atoms were studied, and the J^{pd} is increased with the increased tensile strain, which was used to explain the increased Tc with tensile strain obtained by the DFT results [29]. The similar AFM J^{pd} has also been studied in other 2D magnetic semiconductors [30–32]. In addition, the bond lengths [33,37] and the angles between bonds [34–36] in superexchange paths were studied for some magnetic materials. Our approach is to calculate the FM exchange coupling J defined in Eq. (1) with

TABLE V. The DFT results for the hopping-matrix element $|V_{pd}|$ and energy difference $|E_p - E_d|$ between the 3d orbitals of Cr atoms and the 5p orbitals of the nearest Te atoms in 2D Cr_3Te_6 with lattice variations.

Cr atom	Te atom	Cr orbital	Te orbital	Lattice variation $\Delta a/a$	$\lvert V_{pd}\rvert$ (eV)	$\lvert E_p - E_d\rvert$ (eV)	$\lvert V_{pd}\rvert^4/\lvert E_p - E_d\rvert$ (eV^3)
				−2%	0.5167	0.0931	0.7654
9	3	d_{yz} ↑	p_y ↑	0.00	0.4762	0.0417	1.2618
				2%	0.4389	0.0095	3.9126
				−2%	0.4633	0.1955	0.2358
9	3	d_{xz} ↑	p_y ↑	0.00	0.4248	0.1368	0.2380
				2%	0.3898	0.0785	0.2939
				−2%	0.5166	0.0931	0.7655
10	4	d_{yz} ↑	p_y ↑	0.00	0.4761	0.0418	1.2307
				2%	0.4389	0.0095	3.9015
				−2%	0.1767	0.1885	0.0052
10	4	d_{xz} ↑	p_z ↑	0.00	0.1676	0.1129	0.0070
				2%	0.1583	0.0437	0.0144

the superexchange rule, which has not been quantitatively calculated in the previous theoretical studies.

For the doping magnetic materials, the physical picture might be very different. For example, the carrier-mediated exchange coupling has been discussed in some diluted magnetic semiconductors with high Curie temperatures [53,54]. It could be interesting to develop the current approach to study the doping magnetic systems. The long-range interaction could be important in some magnetic materials. Since the superexchange interaction has been established between the magnetic ions and their nearest neighboring nonmagnetic anions, only the superexchange couplings between the nearest neighboring magnetic ions are studied in our paper. It could be interesting to develop the current approach to study the long-range interactions.

VI. CONCLUSION

Based on the DFT and Wannier function calculations, we propose a procedure for constructing the 2D Heisenberg model with the superexchange interactions. By this approach, we obtain a 2D Heisenberg model with six different nearest-neighbor exchange couplings for the 2D ferromagnetic metal Cr_3Te_6. The calculated Curie temperature Tc = 328 K is close to the Tc = 344 K of Cr_3Te_6 in the experiment. In addition, we predicted two 2D magnetic semiconductors: Cr_3O_6 with band gap of 0.99 eV and Tc = 218 K, and Mn_3O_6 with band gap of 0.75 eV and Tc = 208 K, where the similar 2D Heisenberg models are obtained. The complex Heisenberg model developed from the simple crystal structure shows the power of our approach to study the magnetic properties in these 2D magnetic metals and semiconductors.

ACKNOWLEDGMENTS

This work is supported in part by the National Natural Science Foundation of China (Grants No. 12074378 and No. 11834014), the Beijing Natural Science Foundation (Grant No. Z190011), the National Key R&D Program of China (Grant No. 2018YFA0305800), the Beijing Municipal Science and Technology Commission (Grant No. Z191100007219013), the Chinese Academy of Sciences (Grants No. YSBR-030 and No. Y929013EA2), and the Strategic Priority Research Program of Chinese Academy of Sciences (Grants No. XDB28000000 and No. XDB33000000).

[1] B. Huang, G. Clark, E. Navarro-Moratalla, D. R. Klein, R. Cheng, K. L. Seyler, D. Zhong, E. Schmidgall, M. A. McGuire, D. H. Cobden, W. Yao, D. Xiao, P. Jarillo-Herrero, and X. Xu, Layer-dependent ferromagnetism in a van der Waals crystal down to the monolayer limit, Nature (London) **546**, 270 (2017).

[2] C. Gong, L. Li, Z. Li, H. Ji, A. Stern, Y. Xia, T. Cao, W. Bao, C. Wang, Y. Wang, Z. Q. Qiu, R. J. Cava, S. G. Louie, J. Xia, and X. Zhang, Discovery of intrinsic ferromagnetism in two-dimensional van der Waals crystals, Nature (London) **546**, 265 (2017).

[3] N. Mermin and H. Wagner, Absence of Ferromagnetism or Antiferromagnetism in One- or Two-Dimensional Isotropic Heisenberg Models, Phys. Rev. Lett. **17**, 1307 (1966).

[4] Z. Zhang, J. Shang, C. Jiang, A. Rasmita, W. Gao, and T. Yu, Direct photoluminescence probing of ferromagnetism in monolayer two-dimensional $CrBr_3$, Nano Lett. **19**, 3138 (2019).

[5] X. Cai, T. Song, N. P. Wilson, G. Clark, M. He, X. Zhang, T. Taniguchi, K. Watanabe, W. Yao, D. Xiao, M. A. McGuire, D. H. Cobden, and X. Xu, Atomically thin $CrCl_3$: An in-plane layered antiferromagnetic insulator, Nano Lett. **19**, 3993 (2019).

[6] F. Cui, X. Zhao, J. Xu, B. Tang, Q. Shang, J. Shi, Y. Huan, J. Liao, Q. Chen, Y. Hou, Q. Zhang, S. J. Pennycook, and Y. Zhang, Controlled growth and thickness-dependent conduction-type transition of 2D ferrimagnetic Cr_2S_3 semiconductors, Adv. Mater. **32**, 1905896 (2020).

[7] J. Chu, Y. Zhang, Y. Wen, R. Qiao, C. Wu, P. He, L. Yin, R. Cheng, F. Wang, Z. Wang, J. Xiong, Y. Li, and J. He, Sub-millimeter-scale growth of one-unit-cell-thick ferrimagnetic Cr_2S_3 nanosheets, Nano Lett. **19**, 2154 (2019).

[8] B. Achinuq, R. Fujita, W. Xia, Y. Guo, P. Bencok, G. van der Laan, and T. Hesjedal, Covalent mixing in the 2D ferromagnet $CrSiTe_3$ evidenced by magnetic X-ray circular dichroism, Phys. Status. Solidi. Rapid. Res. Lett. **16**, 2100566 (2022).

[9] K. Lee, A. H. Dismukes, E. J. Telford, R. A. Wiscons, J. Wang, X. Xu, C. Nuckolls, C. R. Dean, X. Roy, and X. Zhu, Magnetic order and symmetry in the 2D semiconductor CrSBr, Nano Lett. **21**, 3511 (2021).

[10] X. Zhao, J. Dong, L. Fu, Y. Gu, R. Zhang, Q. Yang, L. Xie, Y. Tang, and F. Ning, $(Ba_{1-x}Na_x)F(Zn_{1-x}Mn_x)Sb$: A novel fluoride-antimonide magnetic semiconductor with decoupled charge and spin doping, J. Semicond. **43**, 112501 (2022).

[11] J. Zhao, Y. Li, and P. Xiong, A pioneer in magnetic semiconductors – Professor Stephan von Molnár, J. Semicond. **42**, 010302 (2021).

[12] W. Huang, R. Lin, W. Chen, Y. Wang, and H. Zhang, High room-temperature magnetization in Co-doped TiO_2 nanoparticles promoted by vacuum annealing for different durations, J. Semicond. **42**, 072501 (2021).

[13] Z. Sun, B. Cai, X. Chen, W. Wei, X. Li, D. Yang, C. Meng, Y. Wu, and H. Zeng, Prediction and observation of defect-induced room-temperature ferromagnetism in halide perovskites, J. Semicond. **41**, 122501 (2020).

[14] M. Wang, L. Kang, J. Su, L. Zhang, H. Dai, H. Cheng, X. Han, T. Zhai, Z. Liu, and J. Han, Two-dimensional ferromagnetism in CrTe flakes down to atomically thin layers, Nanoscale **12**, 16427 (2020).

[15] L. Meng, Z. Zhou, M. Xu, S. Yang, K. Si, L. Liu, X. Wang, H. Jiang, B. Li, P. Qin, P. Zhang, J. Wang, Z. Liu, P. Tang, Y. Ye, W. Zhou, L. Bao, H.-J. Gao, and Y. Gong, Anomalous thickness dependence of Curie temperature in air-stable two-dimensional ferromagnetic 1T-$CrTe_2$ grown by chemical vapor deposition, Nat. Commun. **12**, 809 (2021).

[16] X. Zhang, Q. Lu, W. Liu, W. Niu, J. Sun, J. Cook, M. Vaninger, P. F. Miceli, D. J. Singh, S.-W. Lian, T.-R. Chang, X. He, J. Du, L. He, R. Zhang, G. Bian, and Y. Xu, Room-temperature intrinsic ferromagnetism in epitaxial $CrTe_2$ ultrathin films, Nat. Commun. **12**, 2492 (2021).

[17] R. Chua, J. Zhou, X. Yu, W. Yu, J. Gou, R. Zhu, L. Zhang, M. Liu, M. B. H. Breese, W. Chen, K. P. Loh, Y. P. Feng, M. Yang, Y. L. Huang, and A. T. S. Wee, Room temperature ferromagnetism of monolayer chromium telluride with perpendicular magnetic anisotropy, Adv. Mater. **33**, 2103360 (2021).

[18] B. Li, X. Deng, W. Shu, X. Cheng, Q. Qian, Z. Wan, B. Zhao, X. Shen, R. Wu, S. Shi, H. Zhang, Z. Zhang, X. Yang, J. Zhang, M. Zhong, Q. Xia, J. Li, Y. Liu, L. Liao, Y. Ye *et al.*, Air-stable ultrathin Cr_3Te_4 nanosheets with thickness-dependent magnetic biskyrmions, Mater. Today **57**, 66 (2022).

[19] Y. Zhang, J. Chu, L. Yin, T. Shifa, Z. Cheng, R. Cheng, F. Wang, Y. Wen, X. Zhan, Z. Wang, and J. He, Ultrathin magnetic 2D single-crystal CrSe, Adv. Mater. **31**, 1900056 (2019).

[20] Z. Fei, B. Huang, P. Malinowski, W. Wang, T. Song, J. Sanchez, W. Yao, D. Xiao, X. Zhu, A. F. May, W. Wu, D. H. Cobden, J.-H. Chu, and X. Xu, Two-dimensional itinerant ferromagnetism in atomically thin itinerant ferromagnetism Fe_3GeTe_2, Nat. Mater. **17**, 778 (2018).

[21] Y. Deng, Y. Yu, Y. Song, J. Zhang, N. Z. Wang, Z. Sun, Y. Yi, Y. Z. Wu, S. Wu, J. Zhu, J. Wang, X. H. Chen, and Y. Zhang, Gate-tunable room-temperature ferromagnetism in two-dimensional Fe_3GeTe_2, Nature (London) **563**, 94 (2018).

[22] J. Seo, D. Kim, E. An, K. Kim, G.-Y. Kim, S.-Y. Hwang, D. Kim, B. Jang, H. Kim, G. Eom, S. Seo, R. Stania, M. Muntwiler, J. Lee, K. Watanabe, T. Taniguchi, Y. Jo, J. Lee, B. Min, M. Jo *et al.*, Nearly room temperature ferromagnetism in a magnetic metal-rich van der Waals metal, Sci. Adv. **6**, eaay8912 (2020).

[23] X. Chen, Y.-T. Shao, R. Chen, S. Susarla, T. Hogan, Y. He, H. Zhang, S. Wang, J. Yao, P. Ercius, D. Muller, R. Ramesh, and R. Birgeneau, Pervasive Beyond Room-Temperature Ferromagnetism in a Doped Van Der Waals Magnet, Phys. Rev. Lett. **128**, 217203 (2022).

[24] A. May, D. Ovchinnikov, Q. Zheng, R. Hermann, S. Calder, B. Huang, Z. Fei, Y. Liu, X. Xu, and M. Mcguire, Ferromagnetism near room temperature in the cleavable van der Waals crystal Fe_5GeTe_2, ACS. Nano. **13**, 4436 (2019).

[25] D. J. O'Hara, T. Zhu, A. H. Trout, A. S. Ahmed, Y. K. Luo, C. H. Lee, M. R. Brenner, S. Rajan, J. A. Gupta, D. W. McComb, and R. K. Kawakami, Room temperature intrinsic ferromagnetism in epitaxial manganese selenide films in the monolayer limit, Nano. Lett. **18**, 3125 (2018).

[26] P. W. Anderson, Antiferromagnetism. theory of superexchange interaction, Phys. Rev. **79**, 350 (1950).

[27] J. B. Goodenough and A. L. Loeb, Theory of ionic ordering, crystal distortion, and magnetic exchange due to covalent forces in spinels, Phys. Rev. **98**, 391 (1955).

[28] J. Kanamori, Theory of the magnetic properties of ferrous and cobaltous oxides, I, Prog. Theor. Phys. **17**, 177 (1957).

[29] X.-J. Dong, J.-Y. You, B. Gu, and G. Su, Strain-Induced Room-Temperature Ferromagnetic Semiconductors with Large Anomalous Hall Conductivity in Two-Dimensional $Cr_2Ge_2Se_6$, Phys. Rev. Appl. **12**, 014020 (2019).

[30] X.-J. Dong, J.-Y. You, Z. Zhang, B. Gu, and G. Su, Great enhancement of Curie temperature and magnetic anisotropy in two-dimensional van der Waals magnetic semiconductor heterostructures, Phys. Rev. B **102**, 144443 (2020).

[31] J.-Y. You, Z. Zhang, X.-J. Dong, B. Gu, and G. Su, Two-dimensional magnetic semiconductors with room Curie temperatures, Phys. Rev. Res. **2**, 013002 (2020).

[32] J.-Y. You, X.-J. Dong, B. Gu, and G. Su, Electric field induced topological phase transition and large enhancements of spin-orbit coupling and Curie temperature in two-dimensional ferromagnetic semiconductors, Phys. Rev. B **103**, 104403 (2021).

[33] S. Chen, C. Huang, H. Sun, J. Ding, P. Jena, and E. Kan, Boosting the Curie temperature of two-dimensional semiconducting CrI_3 monolayer through van der Waals heterostructures, J. Phys. Chem. C **123**, 17987 (2019).

[34] J. He, G. Ding, C. Zhong, S. Li, D. Li, and G. Zhang, Remarkably enhanced ferromagnetism in a super-exchange governed $Cr_2Ge_2Te_6$ monolayer via molecular adsorption, J. Mater. Chem. C **7**, 5084 (2019).

[35] Y. Li, D. Legut, X. Liu, C. Lin, X. Feng, Z. Li, and Q. Zhang, Modulated ferromagnetism and electric polarization induced by surface vacancy in MX_2 monolayers, J. Phys. Chem. C **126**, 8817 (2022).

[36] X. Hu, Y. Zhao, X. Shen, A. V. Krasheninnikov, Z. Chen, and L. Sun, Enhanced ferromagnetism and tunable magnetism in Fe_3GeTe_2 monolayer by strain engineering, ACS Appl. Mater. Interfaces **12**, 26367 (2020).

[37] X. Tang, W. Sun, Y. Gu, C. Lu, L. Kou, and C. Chen, CoB_6 monolayer: A robust two-dimensional ferromagnet, Phys. Rev. B **99**, 045445 (2019).

[38] H. Xiang, C. Lee, H.-J. Koo, X. Gong, and M.-H. Whangbo, Magnetic properties and energy-mapping analysis, Dalton Trans. **42**, 823 (2013).

[39] H. J. Xiang, E. J. Kan, S.-H. Wei, M.-H. Whangbo, and X. G. Gong, Predicting the spin-lattice order of frustrated systems from first principles, Phys. Rev. B **84**, 224429 (2011).

[40] X. Li, H. Yu, F. Lou, J. Feng, M.-H. Whangbo, and H. Xiang, Spin Hamiltonians in magnets: Theories and computations, Molecules **26**, 803 (2021).

[41] J.-Y. You, B. Gu, and G. Su, The p-orbital magnetic topological states on a square lattice, Natl. Sci. Rev. **9**, nwab114 (2022).

[42] G. Kresse and J. Furthmüller, Efficient iterative schemes for *ab initio* total-energy calculations using a plane-wave basis set, Phys. Rev. B **54**, 11169 (1996).

[43] J. P. Perdew, K. Burke, and M. Ernzerhof, Generalized Gradient Approximation Made Simple, Phys. Rev. Lett. **77**, 3865 (1996).

[44] P. Blöchl, Projector augmented-wave method, Phys. Rev. B **50**, 17953 (1994).

[45] J. Heyd, G. Scuseria, and M. Ernzerhof, Hybrid functionals based on a screened Coulomb potential, J. Chem. Phys. **118**, 8207 (2003).

[46] H. Monkhorst and J. Pack, Special points for Brillouin-zone integrations, Phys. Rev. B **13**, 5188 (1976).

[47] A. Togo and I. Tanaka, First principles phonon calculations in materials science, Scr. Mater. **108**, 1 (2015).

[48] A. Mostofi, J. Yates, G. Pizzi, Y.-S. Lee, I. Souza, D. Vanderbilt, and N. Marzari, An updated version of Wannier90: A tool for obtaining maximally-localised Wannier functions, Comput. Phys. Commun. **185**, 2309 (2014).

[49] A. A. Mostofi, J. R. Yates, Y.-S. Lee, I. Souza, D. Vanderbilt, and N. Marzari, Wannier90: A tool for obtaining maximally-localised Wannier functions, Comput. Phys. Commun. **178**, 685 (2008).

[50] See Supplemental Material at http://link.aps.org/supplemental/10.1103/PhysRevB.107.224411 for details on the seven different magnetic configurations.

[51] D. S. Dai and K. M. Qian, *Ferromagnetism*, Vol. 1 (Science Press, Beijing, 2017).

[52] D. Domaretskiy, M. Philippi, M. Gibertini, N. Ubrig, I. Gutiérrez-Lezama, and A. F. Morpurgo, Quenching the bandgap of two-dimensional semiconductors with a perpendicular electric field, Nat. Nanotechnol. **17**, 1078 (2022).

[53] B. Gu and S. Maekawa, Diluted magnetic semiconductors with narrow band gaps, Phys. Rev. B **94**, 155202 (2016).

[54] J.-Y. You, B. Gu, S. Maekawa, and G. Su, Microscopic mechanism of high-temperature ferromagnetism in Fe, Mn, and Cr-doped InSb, InAs, and GaSb magnetic semiconductors, Phys. Rev. B **102**, 094432 (2020).